Geodetic Imaging of Coseismic Slip and Postseismic Afterslip: Sparsity Promoting Methods Applied to the Great Tohoku Earthquake

Geodetic imaging of coseismic slip and postseismic afterslip: Sparsity promoting methods applied to the great Tohoku earthquake

Eileen L. Evans[1] and Brendan J. Meade[1]

Received 13 April 2012; revised 15 May 2012; accepted 17 May 2012; published 15 June 2012.

[1] Geodetic observations of surface displacements during and following earthquakes such as the March 11, 2011 great Tohoku earthquake can be used to constrain the spatial extent of coseismic slip and postseismic afterslip, and characterize the spectrum of earthquake cycle behaviors. Slip models are often regularized by assuming that slip on the fault varies smoothly in space, which may result in the artificial smearing of fault slip beyond physical boundaries. Alternatively, it may be desirable to estimate a slip distribution that is spatially compact and varies sharply. Here we show that sparsity promoting state vector regularization methods can be used to recover slip distributions with sharp boundaries, representing an alternative end-member result to very smooth slip distributions. Using onshore GPS observations at 298 stations during and in the ~2 weeks following the Tohoku earthquake, we estimate a band of coseismic slip between 30 and 50 km depth extending 500 km along strike with a maximum slip of 64 m, corresponding to a minimum magnitude estimate of M_W = 8.8. Our estimate of afterslip is located almost exclusively down-dip of the coseismic rupture, with a transition between 40 and 50 km depth and an equivalent moment magnitude M_W = 8.2. This depth may be interpreted as coincident with the transition from velocity strengthening to velocity weakening frictional behavior, consistent with the upper limit of cold subduction estimates of the thermal structure of the Japan trench. **Citation:** Evans, E. L., and B. J. Meade (2012), Geodetic imaging of coseismic slip and postseismic afterslip: Sparsity promoting methods applied to the great Tohoku earthquake, *Geophys. Res. Lett.*, *39*, L11314, doi:10.1029/2012GL051990.

1. Introduction

[2] The March 11, 2011 great Tohoku earthquake off the east coast of Japan has been the focus of numerous studies to determine the spatial extent of coseismic slip in order to assess the degree to which the earthquake ruptured portions of the subduction zone inferred to be strongly coupled prior to the earthquake, the extent of near trench slip, and the relationship with afterslip following the earthquake. Answering each of these questions requires the solution of an inverse problem where geodetic [*Sato et al.*, 2011; *Kido et al.*, 2011], teleseismic [e.g., *Fujii et al.*, 2011], strong motion [e.g., *Yokota et al.*, 2011], tsunami run-up [*Mori et al.*, 2011], and tsunami waveform and strain gauge [*Fujii et al.*, 2011] observations are used to infer the spatial distribution of fault slip, typically assuming a linear mapping.

[3] Currently there is significant diversity in estimates of coseismic slip. Coseismic slip at or very near the trench has been estimated from GPS offsets [*Loveless and Meade*, 2011; *Pollitz et al.*, 2011], high frequency GPS [*Yue and Lay*, 2011], teleseismic observations [*Fujii et al.*, 2011; *Ide et al.*, 2011], GPS and teleseismic observations [*Simons et al.*, 2011], tsunami observations [*Maeda et al.*, 2011], and joint inversion of GPS, teleseismic, strong motion, and tsunami observations [*Yokota et al.*, 2011]. However, other estimates of the coseismic slip have been interpreted as suggesting little slip along the trench itself based on static GPS offsets [*Ozawa et al.*, 2011; *Miyazaki et al.*, 2011], GPS and tsunami observations [*Simons et al.*, 2011], and joint inversions of GPS, teleseismic, and strong motion observations [*Lee et al.*, 2011; *Koketsu et al.*, 2011]. Estimates of maximum slip range from 18 m [*Loveless and Meade*, 2011] to 60 m [*Simons et al.*, 2011; *Yue and Lay*, 2011].

[4] Variation in coseismic slip estimates also affects our ability to quantify the spatial relationship between coseismic slip and short-term postseismic deformation on the subduction zone interface. A broad region of afterslip following the Tohoku earthquake estimated from 15 days of postseismic GPS observations is centered down-dip of, but largely overlaps with, the coseismic slip estimate [*Ozawa et al.*, 2011]. Afterslip down-dip of coseismic slip has been observed following multiple large earthquakes [*Chlieh et al.*, 2004; *Miyazaki and Larson*, 2008; *Chlieh et al.*, 2007; *Paul et al.*, 2007; *Vigny et al.*, 2011; *Hsu et al.*, 2002], and is often attributed to a transition between velocity weakening behavior and velocity strengthening behavior on the fault [e.g., *Tse and Rice*, 1986; *Marone et al.*, 1991; *Scholz*, 1998]. However, rigorous comparison of slip during and after the Tohoku main shock has been limited by our ability to sharply resolve and compare spatial patterns of coseismic slip and afterslip.

[5] Here we estimate both co- and post-seismic slip distributions using a sparsity promoting solution method to recover sharp boundaries to slip, providing an alternative to smoothed slip estimates. We demonstrate through synthetic resolution tests that sparsity promoting regularization can recover sharp boundaries to slip, and solve for slip during the Tohoku earthquake on an idealized planar array of rectangular dislocation elements [*Okada*, 1985]. We compare

[1]Department of Earth and Planetary Sciences, Harvard University, Cambridge, Massachusetts, USA.

Corresponding author: E. L. Evans, Department of Earth and Planetary Sciences, Harvard University, 20 Oxford St., Cambridge, MA 02138, USA. (elevans@fas.harvard.edu)

sparsity promoting and smoothed estimates of coseismic slip to afterslip in the 15 days following the earthquake, and image a localized band of afterslip directly down-dip of coseismic rupture.

2. Sparsity Promoting Estimation Through ℓ_1 Regularization

[6] The problem of estimating fault slip from geodetic observations is well studied and regularly applied to constrain the rupture extent of large earthquakes. Typically the displacements, **d**, due to slip on fault patches, **m**, are calculated using analytic Green's functions, **G**, for slip on a rectangular dislocation in a homogeneous elastic half space [*Okada*, 1985], forming the linear system $\mathbf{Gm} = \mathbf{d}$. It is often the case that the problem is under-determined (more fault patches than data) and **G** may be poorly conditioned in the sense that some elements lie near the null space and therefore solutions tend to be extremely sensitive to noise in the data. To minimize this sensitivity, a regularization constraint is applied to the state vector, **m** (alternatively, minimizing a cost function containing a term that compares the values of adjacent fault elements [e.g., *Chlieh et al.*, 2007] achieves the same goal), and fault slip estimates are obtained by minimizing the sum of squares of the residual displacements, $\mathbf{Gm} - \mathbf{d}$, along with the constrained state vector, **m** [e.g., *Harris and Segall*, 1987; *Maerten et al.*, 2005]. This may also be written as a damped least squares problem where parameter α is included in the minimization to damp oscillations and drive the state vector toward a common value with increasing α: $\min \|\mathbf{Gm} - \mathbf{d}\|_2 + \alpha\|\mathbf{m}\|_2$.

[7] Absolute value (ℓ_1) regularization approaches designed to recover sparse state vectors have been applied in reflection seismology problems in the last four decades [e.g., *Claerbout and Muir*, 1973; *Santosa and Symes*, 1986], and have been recently applied to teleseismic P wave filtering [*Yao et al.*, 2011]. While this approach introduces a non-linear state vector regularization, optimal solutions can be found using standard quadratic programming approaches [*Boyd and Vandenberghe*, 2004]. Interest in ℓ_1 regularization has increased markedly over the last decade with the development of a theoretical understanding of how it very likely recovers the ℓ_0 pseudo-norm, which gives the number of non-zero elements in the state vector [*Donoho*, 2006; *Candes et al.*, 2006]. A state vector is considered sparse if the total number of non-zero elements is much less than the total number of elements in the state vector, and efficient algorithms now exist to solve problems of the form: $\min \|\mathbf{Gm} - \mathbf{d}\|_2 + \lambda\|\mathbf{m}\|_1$ in which λ controls the sparsity of the state vector. The constrained form of this regularized optimization problem is referred to as the least absolute shrinkage and selection operator (lasso) [*Tibshirani*, 1996],

$$\min \|\mathbf{Gm} - \mathbf{d}\|_2 \text{ subject to } \|\mathbf{m}\|_1 \leq \tau \tag{1}$$

in which the value of τ controls the tradeoff between sparseness of the solution slip distribution and model fit to the data, and which can be solved efficiently using a spectral projected gradient root finding algorithm [*van den Berg and Friedlander*, 2008], which we use here. Applied to earthquake slip distributions, ℓ_1 regularization produces a compact representation of slip, and may be considered an alternative end-member to smoothed ℓ_2 regularized solutions.

3. GPS Data, Model Geometry, and Resolution Tests

[8] We consider 298 onshore coseismic (data from the Geospatial Information Authority of Japan processed by U.S. Jet Propulsion Laboratory: ftp://sideshow.jpl.nasa.gov/pub/users/ARIA) and 15 days of postseismic [*Ozawa et al.*, 2011] GPS observations, including only GPS observation locations that appear in both catalogs to avoid bias due to station location. Due to potential complexities in vertical deformation associated with subduction erosion on the Japan subduction zone [*Heki*, 2004], we consider only the horizontal components of the observations. Seven seafloor observations [*Sato et al.*, 2011; *Kido et al.*, 2011] record the coseismic rupture, however they also contain at least two weeks of the postseismic period as well, and are therefore not included in this comparison. We use simplified representation of the Japan subduction zone parameterized as a planar array of 1000 rectangular dislocation elements [*Okada*, 1985] with dimensions of 700 km along strike and 280 km down-dip. Each rectangular element has dimensions of 196 km^2. The simplified single planar fault dips 15° with a strike of 199° (Figure 1).

[9] To test the ability of sparsity promoting regularization to recover a known slip distribution, we perform a set of resolution tests. Because ℓ_1 regularization methods are designed to recover sparse solutions, the slip distribution used to generate synthetic velocities must also be sparse. Instead of performing a checkerboard resolution test, which requires 50% of the model fault to slip, we impose 30 m of slip on three different subsets of rectangular dislocations. For the resolution tests, the convergence criterion in the spgl1 algorithm [*van den Berg and Friedlander*, 2008] is set to an optimality tolerance of 10^{-4}. A smoothed solution may produce slip estimates that are small, but will rarely be exactly equal to zero. In contrast, sparsity promoting regularization results in a state vector in which most elements are exactly zero. For consistent interpretation of both distributions, we consider recovery of slip less than 50 cm as identifying a non-slipping dislocation. This precludes the interpretation of low magnitude smoothing artifacts that may extend estimated rupture areas significantly.

[10] We impose 30 m of slip on a 9800 km^2 rectangular subset of 50 of the rectangular dislocations (Figure 2a). A forward model of this slip distribution generates synthetic observation displacements. We then invert the synthetic observation displacements to recover the known slip distribution using sparsity promoting regularization as well as damped least squares. In these tests, no synthetic noise is added. ℓ_1 regularized recovery of the slip distribution produces a maximum slip of 36.5 m (τ = 1500), identifies all of the known slipping dislocations, and falsely identifies 15 (2%) of the non-slipping rectangular dislocations (Figure 2b). The damped least squares recovery of the slip distribution produces a maximum slip of 37.7 m ($\alpha = 10^{-8}$), identifies all of the slipping rectangles, but falsely identifies 95 (10%) slipping rectangular dislocations (Figure 2c).

[11] To test recovery of slip as a function of depth, we impose 30 m of slip on a 56 km wide fault patch extending

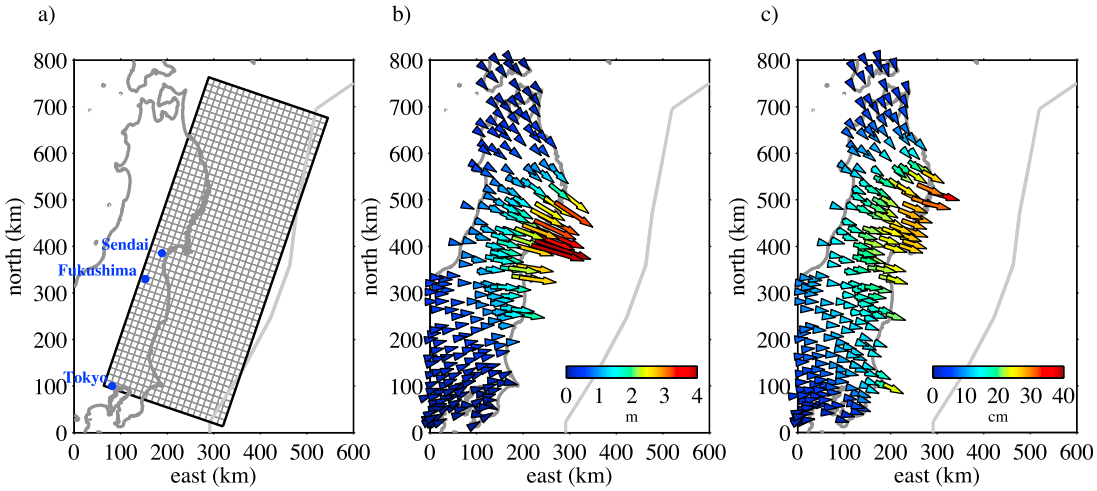

Figure 1. Figure showing model inputs: Japan coastline shown in in dark grey, trench shown in light grey (a) idealized planar fault geometry: strike 199°, dip 15°; (b) coseismic displacements (from the Geospatial Information Authority of Japan processed by U.S. Jet Propulsion Laboratory: ftp://sideshow.jpl.nasa.gov/pub/users/ARIA); (c) postseismic displacements [*Ozawa et al.*, 2011].

from the base of the model fault to the trench made up of 280 rectangular dislocations (Figure 2d). With no synthetic noise, the ℓ_1 regularized recovery of the slip distribution produces a maximum slip of 43.7 m (τ = 2300), identifies all of the known slipping dislocations, and falsely identifies 14 (6%) of the non-slipping rectangular dislocations (Figure 2e). The damped least squares recovery of the slip distribution produces a maximum slip of 38.4 m ($\alpha = 10^{-8}$), identifies all of the slipping rectangles, but falsely identifies 270 (38%) slipping rectangular dislocations (Figure 2f). An additional resolution test is described in Text S2 in the auxiliary material.[1]

[12] In all of the resolution tests, sparsity promoting regularization falsely identifies fewer slipping rectangular dislocations than damped least squares, and is therefore less likely to artificially smear fault slip rates beyond their physical extent. Both regularization methods lose recovery ability with distance from the coast (Figure S5 and Text S2). The most poorly resolved 33% of rectangular dislocations occur shallower than about 20 km depth (Figure S5 and Text S2 and Figures 2 and 3), suggesting slip on the shallowest portion of the subduction zone interface cannot be resolved using onshore GPS data [e.g., *Loveless and Meade*, 2010].

4. Coseismic and Postseismic Slip Distributions

[13] Sparsity promoting estimation of coseismic slip (τ = 1900) identifies a linear trend of 10–60 m slip in a relatively narrow depth range between 20 and 40 km depth and extending 500 km along strike (Figure 3a). To select a τ value, we choose the distribution with the best fit to the data, defined by the smallest mean residual displacement, that still satisfies conditions for a sparse recoverable problem (Text S1) [*Donoho and Tanner*, 2009]. Text S1 contains additional details of determining the value of τ. Due to the presence of observational noise in real geodetic observations, the convergence criterion for the minimization algorithm is relaxed to an optimality tolerance of 8×10^{-3}. This slip distribution results in a mean residual displacement of 0.03 m at the 298 GPS stations (Text S3). We estimate a moment for this distribution of 2.1×10^{22} Nm (assuming shear modulus μ = 58 GPa, calculated from *Nishida et al.* [2008]), and a moment magnitude of M_W = 8.8, which represents a minimum magnitude estimate because slip may occur up-dip of the shallowest slip estimated here, but cannot be recovered with the onshore data.

[14] For comparison, we estimate coseismic slip using underdetermined damped least squares. With a smoothing parameter $\alpha = 10^{-4}$, the area of maximum estimated slip extends about 200 km along strike and is concentrated in the depth range between 30 and 40 km, with a maximum estimated slip of 21 m (Figure 3b). This slip distribution results in a mean residual displacement of 0.02 m (Text S3). We estimate a moment of 2.5×10^{22} Nm and moment magnitude of M_W = 8.9 for the smooth distribution. For consistent interpretation of both regularization methods, as with the resolution tests, we consider recovery of slip greater than 50 cm as identifying a slipping dislocation in both sparsity promoting and damped-least-squares estimates of coseismic slip.

[15] Surface displacements in the postseismic period of the earthquake cycle may be attributed to a combination of afterslip, viscoelastic relaxation, and poroelastic rebound. For simplicity and for direct comparison with coseismic slip, we attribute all postseismic deformation to afterslip, as did *Ozawa et al.* [2011]. Estimated afterslip is therefore a maximum. We estimate ℓ_1 regularized postseismic afterslip with the same process as with coseismic slip, with τ = 230 (Text S1). The sharply varying estimate of afterslip identifies a linear trend of 1–4 m slip down-dip of the coseismic estimate at 40 km depth. Estimated afterslip does not propagate as far as coseismic slip, extending 200 km along strike (Figure 3c). Total estimated afterslip is equivalent to a moment of 2.6×10^{21} Nm, and M_W = 8.2. This slip distribution results in a mean residual displacement of 0.01 m (Text S3).

[16] As with coseismic slip, we also estimate afterslip using underdetermined damped least squares. With a

[1]Auxiliary materials are available in the HTML. doi:10.1029/2012GL051990.

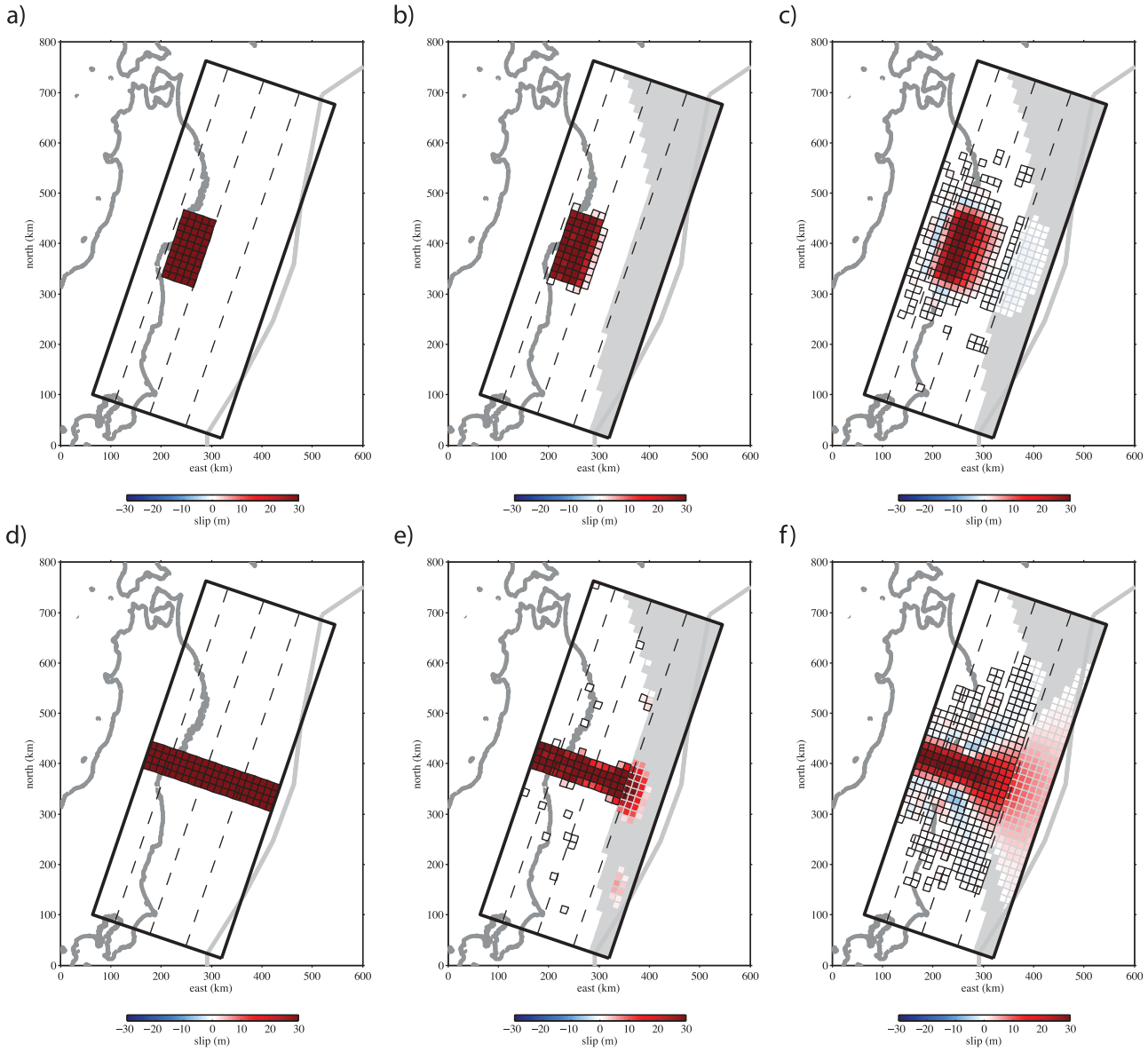

Figure 2. Resolution test demonstrating recovery of a known slip distribution with sparsity promoting and smooth regularization techniques. The 33% least resolved rectangular dislocations shown in gray. (a) Input slip distribution consisting of 30 m of slip on a 9800 km^2 rectangular subset of 50 rectangular dislocations; (b) sparsity promoting recovery of input distribution shown in Figure 2a; (c) damped least squares recovery of input slip distribution show in Figure 2a; (d) input slip distribution with 30 m of slip on a 56 km wide fault patch extending from the base of the model fault to the trench made up of 280 rectangular dislocations; (e) sparsity promoting recovery of input distribution shown in Figure 2d; (f) damped least squares recovery of input slip distribution shown in Figure 2d.

smoothing parameter $\alpha = 10^{-4}$, the area of maximum estimated slip extends about 200 km along strike and is concentrated in the depth range between 30 and 40 km (Figure 3d). We estimate an equivalent moment of 2.3×10^{21}, and $M_W = 8.3$. This slip distribution results in a mean residual displacement of 0.01 m (Text S3). For afterslip distributions, we consider recovery of slip greater than 20 cm as identifying a slipping dislocation in both sparsity promoting and damped-least-squares estimates of afterslip.

5. Discussion

[17] We estimate postseismic afterslip following the Tohoku earthquake almost completely down-dip of and distinct from the region of coseismic slip. To directly compare the sharply varying estimates of coseismic and postseismic slip, we identify the largest contiguous slipping patches in both distributions (Figure 3e). The two regimes are largely distinct from one another, overlapping at 13 rectangular dislocations (1% of the total modeled fault surface area). Overlap between the lower extent of contiguous coseismic slip and the upper bound of postseimic afterslip occurs between 40 and 50 km depth. This afterslip distribution is in contrast to the distribution estimated by *Ozawa et al.* [2011], where afterslip spans a broad region of the fault and almost completely overlaps with the region of estimated coseismic rupture. Our smoothed distributions of

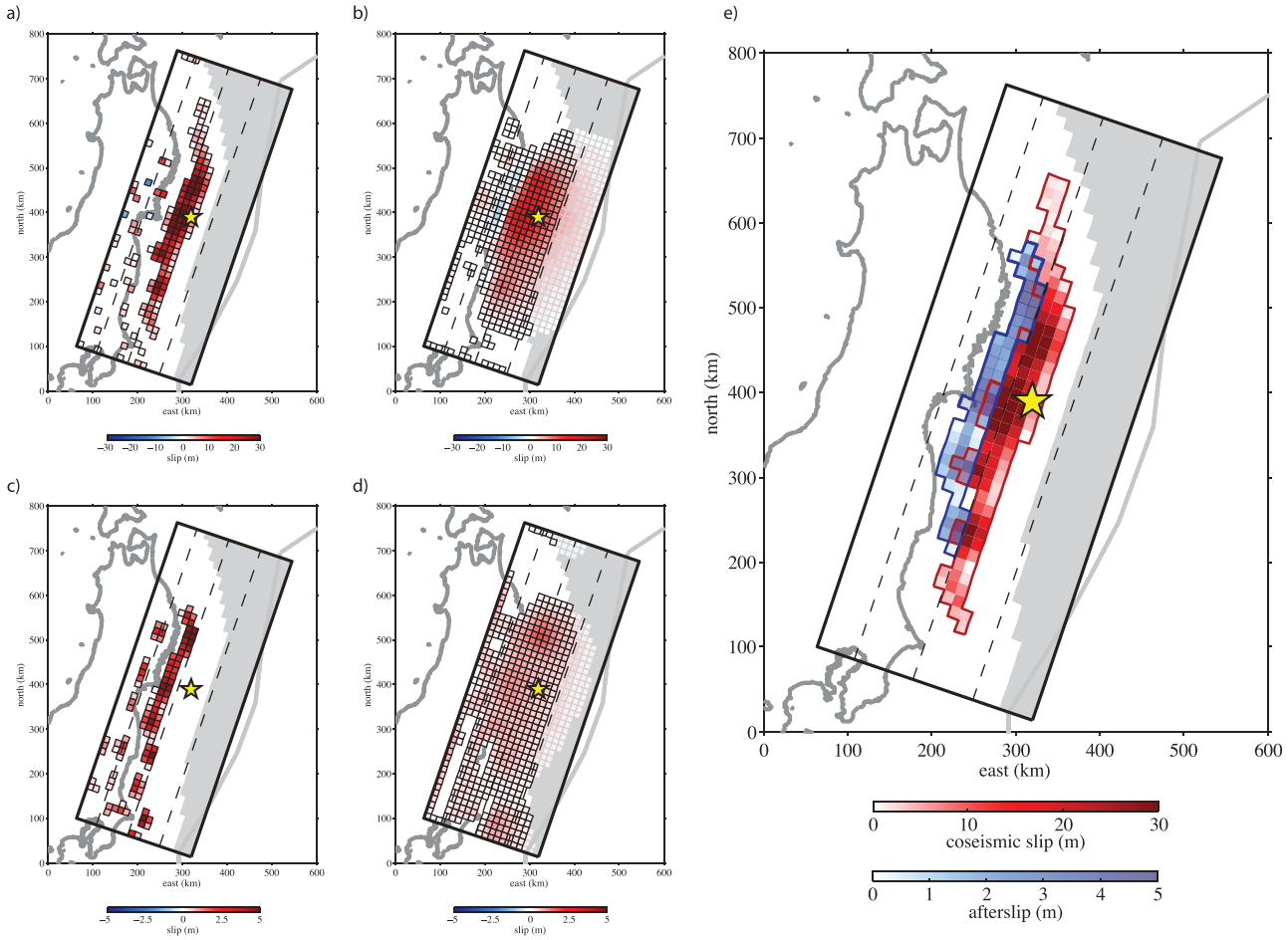

Figure 3. Comparison of sparsity promoting and smooth regularization methods for coseismic slip and postseismic afterslip. The 33% least resolved rectangular dislocations shown in gray. Epicenter location shown by yellow star. (a) Sparsity promoting estimate of coseismic slip; (b) damped least squares estimate of coseismic slip; (c) sparsity promoting estimate of postseismic afterslip; (d) damped least squares estimate of postseismic afterslip; (e) combined coseismic and postseismic slip: largest contiguous coseismic slipping region shown in red, and largest contiguous postseismic region shown in blue. The distributions overlap in 13 rectangular dislocations between 40 and 50 km depth.

co- and post-seismic slip estimated with damped least squares are consistent with the spatial extent of slip estimated by *Ozawa et al.* [2011], in which smoothness is imposed by damping roughness within a Bayesian framework [*Yabuki and Matsu'ura*, 1992]. These smooth distributions limit the identification of a potentially sharp mechanical boundary between the two regimes. Although neither coseismic nor postseismic slip distribution extends more shallowly than 25 km depth, we do not suggest the absence of updip slip, only that onshore geodetic data alone are insufficient to uniquely resolve near trench behavior (Text S2) [*Loveless and Meade*, 2010].

[18] The spatial distinction between regions of coseismic and postseismic slip may be attributed to a transition from velocity weakening frictional properties, where earthquakes nucleate, to velocity strengthening frictional properties that allow for stable sliding [e.g., *Tse and Rice*, 1986; *Marone et al.*, 1991; *Scholz*, 1998]. Rock friction experiments on gabbro [*He et al.*, 2007], and granite gouge [*Blanpied et al.*, 1995] suggest a temperature controlled transition from velocity weakening to velocity strengthening behavior at 250–300°C. Using a temperature profile model of the subduction zone off the coast of Tohoku [*Peacock and Wang*, 1999] the lower transition from velocity weakening to velocity strengthening should occur at 65 km depth, over 20 km deeper than the imaged transition between co- and post-seismic slip. To demonstrate a potential application of sharply resolved slip distributions, we use the imaged transition zone depth to modify the temperature profile on the subduction zone. The modified temperature profile is within the 50–100°C uncertainty in the *Peacock and Wang* [1999] above 50 km, and the modified a-b profile predicts velocity weakening in the depth range of 18–43 km (Figure 4).

6. Conclusion

[19] Sparsity promoting estimation techniques can recover compact and sharply varying slip distributions that fit geodetic observations as well as smoothed distributions, and allow quantitative assessment of the spatial relationship between coseismic slip and the rest of the earthquake cycle. Sparsity promoting estimates of slip in the great Tohoku earthquake identify a linear trend of slip between 20 and 40 km depth with a maximum coseismic slip of 64 m, and a narrow transition zone between coseismic slip and postseismic afterslip at depths of 40–50 km. Interpreted as a

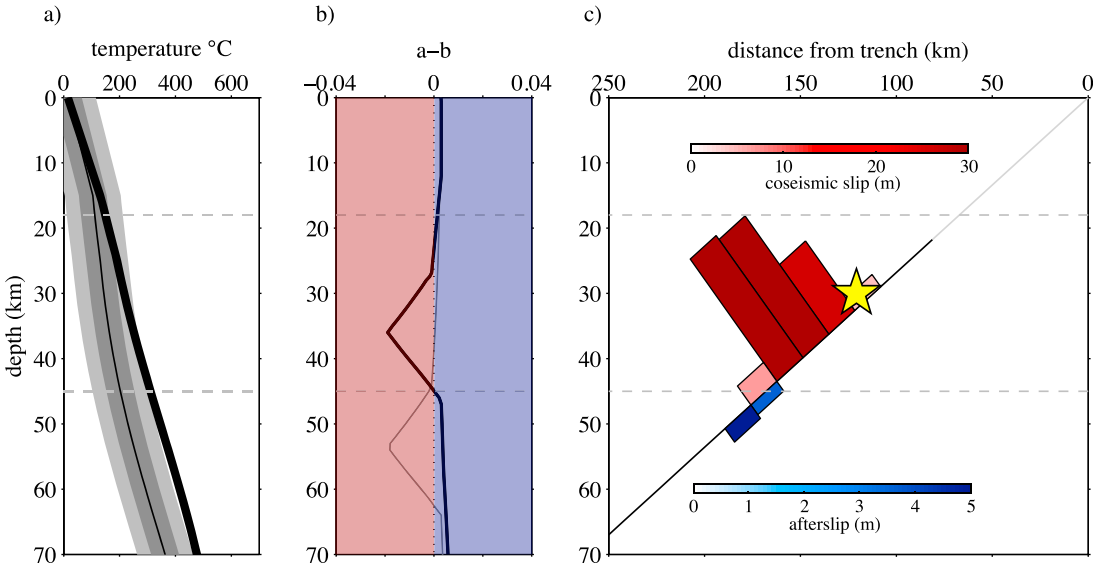

Figure 4. (a) Temperature profile ±50 and 100 C from *Peacock and Wang* [1999], and temperature profile based on modified a–b profile (thick black line); (b) a–b from *He et al.* [2007], calculated from temperature profile of *Peacock and Wang* [1999] (grey line) and adjusted based on transition between coseismic slip and postseismic afterslip (black line) negative a–b values are velocity weakening (pink), and positive a–b values are velocity strengthening (blue); (c) cross section of model fault surface showing slip rates and hypocenter (yellow star). Dashed gray lines represent predicted region of velocity weakening. The updip portion of the fault is shown in gray where resolution is limited.

transition in idealized temperature-dependent frictional behavior from velocity weakening to velocity strengthening, this depth range is consistent with the warmest limit of estimated temperature profiles of the Japan trench subduction zone. In this sense, the ability to image sharp boundaries to co- and post-seismic slip provides new images of earthquake cycle processes that may be used constrain the thermal structure of subduction zones and the depth profile of frictional behavior.

[20] **Acknowledgments.** We thank the Associate Editor and two anonymous reviewers for their thoughtful comments that improved the quality of this paper.

[21] The Editor thanks two anonymous reviewers for assisting in the evaluation of this paper.

References

Blanpied, M. L., D. A. Lockner, and J. D. Byerlee (1995), Frictional slip of granite at hydrothermal conditions, *J. Geophys. Res.*, *100*(B7), 13,045–13,064, doi:10.1029/95JB00862.

Boyd, S., and L. Vandenberghe (2004), *Convex Optimization*, Cambridge University Press, Cambridge, UK.

Candes, E. J., J. K. Romberg, and T. Tao (2006), Stable signal recovery from incomplete and inaccurate measurements, *Commun. Pure Appl. Math.*, *59*(8), 1207–1223, doi:10.1002/cpa.20124.

Chlieh, M., J. B. de Chabalier, J. C. Ruegg, R. Armijo, R. Dmowska, J. Campos, and K. L. Feigl (2004), Crustal deformation and fault slip during the seismic cycle in the north Chile subduction zone, from GPS and InSAR observations, *Geophys. J. Int.*, *158*(2), 695–711, doi:10.1111/j.1365-246X.2004.02326.x.

Chlieh, M., et al. (2007), Coseismic slip and afterslip of the great M_W 9.15 Sumatra-Andaman earthquake of 2004, *Bull. Seismol. Soc. Am.*, *97*(1), S152–S173, doi:10.1785/0120050631.

Claerbout, J. F., and F. Muir (1973), Robust modeling with erratic data, *Geophysics*, *38*(5), 826–844, doi:10.1190/1.1440378.

Donoho, D. L. (2006), For most large underdetermined systems of equations, the minimal l(1)-norm near-solution approximates the sparsest near-solution, *Commun. Pure Appl. Math.*, *59*(7), 907–934, doi:10.1002/cpa.20131.

Donoho, D., and J. Tanner (2009), Observed universality of phase transitions in high-dimensional geometry, with implications for modern data analysis and signal processing, *Philosophical Transactions of the Royal Society a-Mathematical Physical and Engineering Sciences*, *367*(1906), 4273–4293.

Fujii, Y., K. Satake, S. Sakai, M. Shinohara, and T. Kanazawa (2011), Tsunami source of the 2011 off the Pacific coast of Tohoku earthquake, *Earth Planets Space*, *63*(7), 815–820, doi:10.5047/eps.2011.06.010.

Harris, R. A., and P. Segall (1987), Detection of a locked zone at depth on the Parkfield, California, segment of the San Andreas fault, *J. Geophys. Res.*, *92*(B8), 7945–7962, doi:10.1029/JB092iB08p07945.

He, C., Z. Wang, and W. Yao (2007), Frictional sliding of gabbro gouge under hydrothermal conditions, *Tectonophysics*, *445*(3–4), 353–362, doi:10.1016/j.tecto.2007.09.008.

Heki, K. (2004), Space geodetic observation of deep basal subduction erosion in northeastern Japan, *Earth Planet. Sci. Lett.*, *219*(1–2), 13–20, doi:10.1016/S0012-821X(03)00693-9.

Hsu, Y. J., N. Bechor, P. Segall, S. B. Yu, L. C. Kuo, and K. F. Ma (2002), Rapid afterslip following the 1999 Chi-Chi, Taiwan earthquake, *Geophys. Res. Lett.*, *29*(16), 1754, doi:10.1029/2002GL014967.

Ide, S., A. Baltay, and G. C. Beroza (2011), Shallow dynamic overshoot and energetic deep rupture in the 2011 M_W 9.0 Tohoku-Oki earthquake, *Science*, *332*(6036), 1426–1429, doi:10.1126/science.1207020.

Kido, M., Y. Osada, H. Fujimoto, R. Hino, and Y. Ito (2011), Trench-normal variation in observed seafloor displacements associated with the 2011 Tohoku-Oki earthquake, *Geophys. Res. Lett.*, *38*, L24303, doi:10.1029/2011GL050057.

Koketsu, K., et al. (2011), A unified source model for the 2011 Tohoku earthquake, *Earth Planet. Sci. Lett.*, *310*(3–4), 480–487, doi:10.1016/j.epsl.2011.09.009.

Lee, S.-J., B.-S. Huang, M. Ando, H.-C. Chiu, and J.-H. Wang (2011), Evidence of large scale repeating slip during the 2011 Tohoku-Oki earthquake, *Geophys. Res. Lett.*, *38*, L19306, doi:10.1029/2011GL049580.

Loveless, J. P., and B. J. Meade (2010), Geodetic imaging of plate motions, slip rates, and partitioning of deformation in Japan, *J. Geophys. Res.*, *115*, B02410, doi:10.1029/2008JB006248.

Loveless, J. P., and B. J. Meade (2011), Spatial correlation of interseismic coupling and coseismic rupture extent of the 2011 M_W = 9.0 Tohoku-oki earthquake, *Geophys. Res. Lett.*, *38*, L17306, doi:10.1029/2011GL048561.

Maeda, T., T. Furumura, S. I. Sakai, and M. Shinohara (2011), Significant tsunami observed at ocean-bottom pressure gauges during the 2011 off the Pacific coast of Tohoku earthquake, *Earth Planets Space*, *63*(7), 803–808, doi:10.5047/eps.2011.06.005.

Maerten, F., P. Resor, D. Pollard, and L. Maerten (2005), Inverting for slip on three-dimensional fault surfaces using angular dislocations, *Bull. Seismol. Soc. Am.*, *95*(5), 1654–1665, doi:10.1785/0120030181.

Marone, C. J., C. H. Scholtz, and R. Bilham (1991), On the mechanics of earthquake afterslip, *J. Geophys. Res.*, *96*(B5), 8441–8452, doi:10.1029/91JB00275.

Miyazaki, S., and K. M. Larson (2008), Coseismic and early postseismic slip for the 2003 Tokachi-oki earthquake sequence inferred from GPS data, *Geophys. Res. Lett.*, *35*, L04302, doi:10.1029/2007GL032309.

Miyazaki, S., J. J. McGuire, and P. Segall (2011), Coseismic and aseismic fault slip before and during the 2011 off the Pacific coast of Tohoku earthquake, *Earth Planets Space*, *63*(7), 637–642, doi:10.5047/eps.2011.07.001.

Mori, N., T. Takahashi, T. Yasuda, and H. Yanagisawa (2011), Survey of 2011 Tohoku earthquake tsunami inundation and run-up, *Geophys. Res. Lett.*, *38*, L00G14, doi:10.1029/2011GL049210.

Nishida, K., H. Kawakatsu, and K. Obara (2008), Three-dimensional crustal *S* wave velocity structure in Japan using microseismic data recorded by Hi-net tiltmeters, *J. Geophys. Res.*, *113*, B10302, doi:10.1029/2007JB005395.

Okada, Y. (1985), Surface deformation due to shear and tensile faults in a half-space, *Bull. Seismol. Soc. Am.*, *75*(4), 1135–1154.

Ozawa, S., T. Nishimura, H. Suito, T. Kobayashi, M. Tobita, and T. Imakiire (2011), Coseismic and postseismic slip of the 2011 magnitude-9 Tohoku-Oki earthquake, *Nature*, *475*(7356), 373–376, doi:10.1038/nature10227.

Paul, J., A. R. Lowry, R. Bilham, S. Sen, and R. Smalley Jr. (2007), Post-seismic deformation of the Andaman Islands following the 26 December, 2004 Great Sumatra-Andaman earthquake, *Geophys. Res. Lett.*, *34*, L19309, doi:10.1029/2007GL031024.

Peacock, S. M., and K. Wang (1999), Seismic consequences of warm versus cool subduction metamorphism: Examples from southwest and northeast Japan, *Science*, *286*(5441), 937–939, doi:10.1126/science.286.5441.937.

Pollitz, F. F., R. Bürgmann, and P. Banerjee (2011), Geodetic slip model of the 2011 M9.0 Tohoku earthquake, *Geophys. Res. Lett.*, *38*, L00G08, doi:10.1029/2011GL048632.

Santosa, F., and W. W. Symes (1986), Linear inversion of band-limited reflection seismograms, *SIAM J. Sci. Stat. Comput.*, *7*(4), 1307–1330, doi:10.1137/0907087.

Sato, M., T. Ishikawa, N. Ujihara, S. Yoshida, M. Fujita, M. Mochizuki, and A. Asada (2011), Displacement above the hypocenter of the 2011 Tohoku-Oki earthquake, *Science*, *332*(6036), 1395, doi:10.1126/science.1207401.

Scholz, C. H. (1998), Earthquakes and friction laws, *Nature*, *391*(6662), 37–42, doi:10.1038/34097.

Simons, M., et al. (2011), The 2011 magnitude 9.0 Tohoku-Oki earthquake: Mosaicking the megathrust from seconds to centuries, *Science*, *332*(6036), 1421–1425, doi:10.1126/science.1206731.

Tibshirani, R. (1996), Regression shrinkage and selection via the Lasso, *J. R. Stat. Soc., Ser. B*, *58*(1), 267–288.

Tse, S. T., and J. R. Rice (1986), Crustal earthquake instability in relation to the depth variation of frictional slip properties, *J. Geophys. Res.*, *91*(B9), 9452–9472, doi:10.1029/JB091iB09p09452.

van den Berg, E., and M. P. Friedlander (2008), Probing the Pareto frontier for basis pursuit solutions, *SIAM J. Sci. Comput.*, *31*(2), 890–912, doi:10.1137/080714488.

Vigny, C., et al. (2011), The 2010 M_W 8.8 Maule megathrust earthquake of central Chile, monitored by GPS, *Science*, *332*(6036), 1417–1421, doi:10.1126/science.1204132.

Yabuki, T., and M. Matsu'ura (1992), Geodetic data inversion using a Bayesian information criterion for spatial distribution of fault slip, *Geophys. J. Int.*, *109*(2), 363–375, doi:10.1111/j.1365-246X.1992.tb00102.x.

Yao, H., P. Gerstoft, P. M. Shearer, and C. Mecklenbräuker (2011), Compressive sensing of the Tohoku-Oki Mw 9.0 earthquake: Frequency-dependent rupture modes, *Geophys. Res. Lett.*, *38*, L20310, doi:10.1029/2011GL049223.

Yokota, Y., K. Koketsu, Y. Fujii, K. Satake, S. Sakai, M. Shinohara, and T. Kanazawa (2011), Joint inversion of strong motion, teleseismic, geodetic, and tsunami datasets for the rupture process of the 2011 Tohoku earthquake, *Geophys. Res. Lett.*, *38*, L00G21, doi:10.1029/2011GL050098.

Yue, H., and T. Lay (2011), Inversion of high-rate (1 sps) GPS data for rupture process of the 11 March 2011 Tohoku earthquake (M_w 9.1), *Geophys. Res. Lett.*, *38*, L00G09, doi:10.1029/2011GL048700.